Chapter 8

Discrete-Time Sliding Mode Controller For Magnetic Levitation System Using Minima Operator

8.1 Introduction

Magnetic levitation systems (MLS) are versatile in their engineering applications, spanning a wide range of industries and technologies. Magnetic levitation offers an intriguing scenario for exploring nonlinear unstable dynamics and crafting corresponding control strategies. The system aims to elevate objects to a specific height by magnetizing the coil, employing the principle of non-contact. Previous studies have explored the control design using feedback linearization techniques [70] and [71], PID control [52], adaptive control [72], robust control [73] and using neural networks based control [74]. Additionally, continuous sliding mode control (CSMC) strategies, known for their robustness compared to other feedback techniques, have been implemented in MLS [75]- [76].

The levitation dynamics display inherent instability characterized by open-loop nonlinear behavior. The objective of the control law introduced in [77] was to minimize the power consumption of the magnetic suspension system. Research in [78] has investigated magnetically levitated conveyors. Additionally, [79] outlines the design of an estimator employing variable structure systems principles. The majority of controllers developed thus far for MLS, including CSMCs, have been in continuous time. very few works [76], [80]- [81], have been reported for discrete control of MLS.

In this chapter, we have developed a DSMC for MLS utilizing RLs [2]. Subsequently, we compared the developed results with previous results. This approach proves more practical for MLS compared to previous methods, chattering associated with quasi sliding mode domain reduces its practical implementation. Our simulation results validate the effectiveness of the minimum operator-based DSMC for magnetic levitation system control.

8.2 System Description

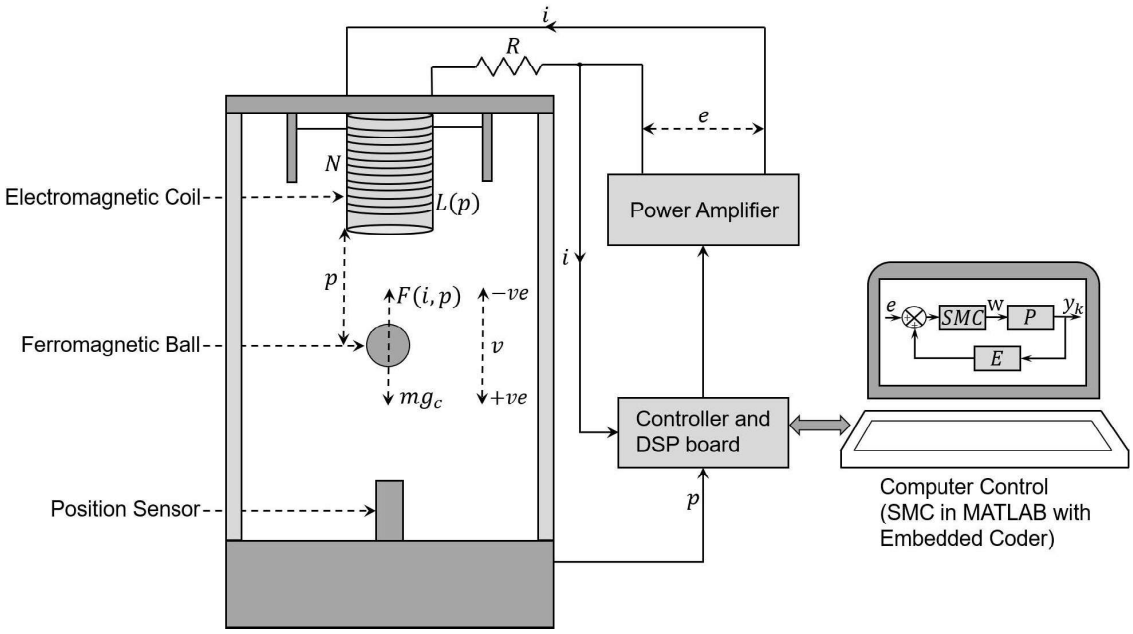

Figure 8.1: Schematic of a MLS

The illustrated MLS, depicted in Fig 8.1, consists of a sphere exhibiting ferromagnetic properties, which is suspended within a magnetic field generated by an electromagnet. This configuration allows the electromagnet to exert an attractive force on the ferromagnetic sphere, counteracting the force of gravity and thus keeping the sphere at a predetermined elevation. The governing equation of this system is delineated below.

$$\begin{aligned} &\frac{dp}{dt} = v, Ri + \frac{d(L(p)i)}{dt} = e, m\frac{dv}{dt} = mg_c - F(i,p) \\ &F(i,p) = Q\left(\frac{i}{p}\right)^2, Q = \frac{\mu_0 A N^2}{4}, L(p) = L_1 + \frac{2Q}{p} \end{aligned} \tag{8.1}$$

The following variables are assigned as: $p = x_1$ (representing the position of the ball),

$v = x_2$ (representing the velocity of the ball), $i = x_3$ (denoting the current in the coil), R (indicating the resistance of the coil), L (referring to the inductance of the coil), g_c = gravitational constant, Q = magnetic force constant, and m = mass of the ball also, L_1 denotes the parameter related to electromagnetic coil inductance.

Therefore, the dynamic formulation of the MLS model (8.1) can be expressed in the guise of nonlinear dynamics as follows:

$$\begin{aligned} \dot{x} &= f(x) + g(x)u \\ y &= h(x) \end{aligned} \tag{8.2}$$

Considering the state vector x as $[x_1, x_2, x_3]^T$ where, $x_1 = p, x_2 = v, x_3 = i$, input as u and output y, the state-space model of the MLS will be expressed as :

$$\begin{aligned} \frac{dx_1}{dt} = x_2, \frac{dx_2}{dt} &= g - \frac{Q}{m}(\frac{x_3}{x_1})^2 \\ \frac{x_3}{dt} &= -\frac{R}{L}x_3 + \frac{2Q}{L}(x_2\frac{x_3}{(x_1)^2}) + \frac{u}{L} \end{aligned} \tag{8.3}$$

The control strategies aim to guide the variables x_1, x_2, and x_3 towards their target equilibrium values x_{1d}, x_{2d}, and x_{3d}, correspondingly where x_{3d} satisfies $x_{3d} = x_{1d}\sqrt{\frac{gm}{Q}}$.

8.2.1 Discrete Linear Model of the MLS

The nonlinear representation of the MLS provided in equation (8.2) undergoes precise linearization through a feedback linearizing transformation.
Consider the transformation $z = \left(z_1, z_2, z_3\right)^T$ as:

$$z = T(x) = \begin{bmatrix} x_1 - x_{1d} \\ x_2 \\ g - \frac{Q/m \cdot (x_3/x_1)^2}{1} \end{bmatrix} \tag{8.4}$$

The system in the form of state space will be as follows:

$$\dot{z} = \begin{bmatrix} \dot{z_1} \\ \dot{z_2} \\ \dot{z_3} \end{bmatrix} = \begin{bmatrix} z_2 \\ z_3 \\ \alpha(z) + \theta(z)u \end{bmatrix} \tag{8.5}$$

where,

$$\begin{aligned} \alpha(z) &= 2\left(g - z_3\right)\left(\left(1 - \frac{2Q}{L(z_1 + x_1 d)}\right)\frac{z_2}{z_1 + x_{1d}} + \frac{R}{L}\right) \\ \theta(z) &= -\frac{2Q}{L(z_1 + x_1 d)}\left(\sqrt{\frac{Q}{m}\left(g - z_3\right)}\right). \end{aligned} \tag{8.6}$$

Table 8.1: Parameters of the MLS.

Parameter	Symbol	Value
Coil resistance	R	28.7 Ω
Coil inductance	L1	0.65 H
Gravitational constant	g	9.81 m/sec^2
Magnetic force constant	Q	1.8 $\times 10^{-4}$
Levitated object mass	m	11.87 $\times 10^{-3} Kg$
Plant initial condition	x1	0.0255 m
	x2	0 m/sec
	x3	1.1 A
Desired steady state values		
	x1d	0.01 m
	x2d	0 m/sec
	x3d	0.2884 A

To nullify the nonlinear elements in equation (8.5), the design of the outer-loop feedback controller u takes the following form:

$$u = -\theta^{-1}(z)(\alpha(z) + v) \tag{8.7}$$

where v represents the inner-loop feedback controller. Therefore, the magnetic levitation system's nonlinear model (8.2) can be expressed as after the application of control input (8.7),

$$\dot{z} = Az + Bu \quad y = Cz; \tag{8.8}$$

where

$$A = \begin{pmatrix} 0 & 1 & 0 \\ 0 & 0 & 1 \\ 0 & 0 & 0 \end{pmatrix}; \quad B = \begin{pmatrix} 0 \\ 0 \\ 1 \end{pmatrix}; \quad C = \begin{pmatrix} 1 & 0 & 0 \end{pmatrix}.$$

The linear model undergoes discretization with a sampling time of $\tau = 0.1$ seconds. Consequently, the continuous-time system described in (8.8) is transformed into a discrete-time system (DTS) is as follows:

$$z(k+1) = \Phi z(k) + \Gamma u(k) \quad y(k) = C\Phi z(k); \tag{8.9}$$

where the state $z(k) \in \mathbb{R}^3$, the input $u(k) \in \mathbb{R}$, and the output $y(k) \in \mathbb{R}$. Moreover, $\Phi = e^{A\tau} \in \mathbb{R}^{3\times3}$, $\Gamma = A^{-1}(e^{A\tau} - I) \in \mathbb{R}^{3\times1}$ and $C \in \mathbb{R}^{1\times3}$. the DTS matrices are as follows:

$$\Phi = \begin{pmatrix} 1 & 0.1 & 0.005 \\ 0 & 1 & 0.1 \\ 0 & 0 & 1 \end{pmatrix}; \quad \Gamma = \begin{pmatrix} 0.0002 \\ 0.005 \\ 0.1 \end{pmatrix}.$$

After the discretization of the system model.

8.3 DSMC For MLS

The switching function is defined as $\aleph(k) := \rho(z(k))$, and the corresponding sliding manifold is defined by the level set $\rho^{-1}(0) := \{z \in D : \rho(z) = 0\}$. For analytical purposes, the switching function is defined as follows:

$$\aleph(k) = c^T z(k), \tag{8.10}$$

where $c \in \mathbb{R}^{n\times1}$ with $c^T\Gamma \neq 0$.

RL1 for DTS

$$\aleph(k+1) = \aleph(k) - \text{sign}[\aleph(k)] \min(|\aleph(k)|, \omega) \tag{8.11}$$

RL2 for DTS

$$\aleph(k+1) = \aleph(k) - \omega\text{sign}[\aleph(k)] \min\left(\frac{|\aleph(k)|}{\omega}, |\aleph(k)|^\beta\right) \tag{8.12}$$

8.3.1 Controller Design Based on RL1

Using switching function (8.10),

$$\aleph(k+1) = c^T z(k+1),$$

consider the system described by (8.9) and RL1 (8.11).

$$c^T(\Phi z(k) + \Gamma u(k)) = \aleph(k) - \text{sign}[\aleph(k)] \min(|\aleph(k)|, \omega)$$

Now, the control input will be expressed as

$$u(k) = -(c^T\Gamma)^{-1}\left(c^T\Phi z(k) \quad -\aleph(k) + \text{sign}[\aleph(k)]\min(|\aleph(k)|, \omega)\right) \tag{8.13}$$

Theorem 8.1 *Consider system* (8.9) *and RL* (8.11)*, using control input* (8.13) *the absolute value of the switching function of the system goes to zero for some* $t \geq I(\aleph_0)$ *where* $I(\aleph_0) = \frac{|\aleph_0|}{\omega}$ *is the settling time function (STF).*

Proof When the control input obtained from equation (8.13) is implemented within the system (8.9), the system adheres to the RL1.

$$\aleph(k+1) = \aleph(k) - \text{sign}[\aleph(k)]\min(|\aleph(k)|, \omega)$$

Consider the scenario where $|\aleph(0)| \leq \omega$, then $\aleph(k+1) = 0$ implies in the next step $|\aleph(k+1)| = 0$. Consequently, $|\aleph(k+1)| = 0$, with $I(\aleph_0) = 1$. Moreover, for all $k \geq I(\aleph_0)$, $|\aleph(k)| = 0$, demonstrating the existence of QSM. For another scenario, if $|\aleph(0)| > \omega$, then $|\aleph(k+1)| = |\aleph(k) - \omega\text{sign}[\aleph(k)]$. As $|\aleph(k)| > \omega$, it follows that $|\aleph(k+1)| \leq |\aleph(k)| - \omega$. Additionally, it can be deduced as:

$$\begin{aligned}
|\aleph(k)| &\leq |\aleph(k-1)| - \omega \\
&\leq |\aleph(k-2)| - 2\omega \\
&\leq \\
&\vdots \\
&\leq |\aleph(0)| - t\omega
\end{aligned}$$

If $(|\aleph(0)| - t\omega) \leq \omega$, then $|\aleph(k)| \leq \omega$, implying $|\aleph(k+1)| = 0$ for all $t \geq \frac{|\aleph_0|-}{\omega}$. The STF is $I(\aleph_0) = \frac{|\aleph_0|}{\omega}$. Therefore, $|\aleph(k)| = 0$ assures within finite time steps.

8.3.2 Controller Design Based on RL2

Using switching function (8.10),

$$\aleph(k+1) = c^T z(k+1),$$

consider the system described by (8.9) and RL2 (8.12).

$$c^T(\Phi z(k) + \Gamma u(k)) = \aleph(k) - \gamma_1 \text{sign}[\aleph(k)]\min\left(\frac{|\aleph(k)|}{\gamma_1}, |\aleph(k)|^\beta\right)$$

Now, the control input will be expressed as

$$u(k) = -(c^T\Gamma)^{-1}\left(c^T\Phi z(k) \quad -\aleph(k) + \gamma_1 \text{sign}[\aleph(k)] \min\left(\frac{|\aleph(k)|}{\gamma_1}, |\aleph(k)|^\beta\right)\right) \tag{8.14}$$

Theorem 8.2 *Consider system* (8.9) *and RL* (8.12)*. If* $\frac{|\aleph(0)|}{\gamma_1} \leq |\aleph(0)|^\beta$ *with* $\gamma_1 \in (0,1)$ *and* $\beta > 0$*, using control input* (8.14)*, the absolute value of the switching function of the system goes to zero for some* $t \geq I(\aleph_0)$*, where* $I(\aleph_0) \leq \left\lceil \log_{[1-\gamma_1|\aleph_0|^{\beta-1}]} \frac{\gamma_1^{\frac{1}{1-\beta}}}{|\aleph_0|} \right\rceil + 1$.

Proof When the control input obtained from equation (8.14) is implemented within the system (8.9), the system adheres to the RL2:

$$\aleph(k+1) = \aleph(k) - \gamma_1 \text{sign}[\aleph(k)] \min\left(\frac{|\aleph(k)|}{\gamma_1}, |\aleph(k)|^\beta\right).$$

Given the simplistic scenario, if $\frac{|\aleph(0)|}{\gamma_1} \leq |\aleph(0)|^\beta$, then

$$\begin{aligned} &\aleph(k+1) = \aleph(k) - \text{sign}[\aleph(k)]|\aleph(k)| \\ &\Rightarrow \aleph(k+1) = 0 \end{aligned}$$

In the subsequent time step. Hence, we obtain
$|\aleph(k+1)| = 0$, with $I(\aleph_0) = 1$. Also, for all $t \geq I(\aleph_0)$, $|\aleph(k+1)| = 0$, showcasing the sliding reaching existence. Taking into account the following scenario, if $\frac{|\aleph(0)|}{\gamma_1} > |\aleph(0)|^\beta$, then

$$\aleph(k+1) = \aleph(k) - \gamma_1 \text{sign}[\aleph(k)]|\aleph(k)|^\beta.$$

We can express it as,

$$|\aleph(k+1)| = |\aleph(k) - \gamma_1 \text{sign}[\aleph(k)]|\aleph(k)|^\beta.$$

Since $|\aleph(k)| > |\aleph(k)|^\beta$, it follows that,

$$|\aleph(k+1)| \leq |\aleph(k)| - \gamma_1|\aleph(k)|^\beta.$$

Further, it can be written as

$$\begin{aligned} |\aleph(k)| &\leq |\aleph(k-1)|(1-\gamma_1|\aleph(k-1)|^{\beta-1}) \\ &\vdots \\ &\leq |\aleph(0)|(1-\gamma_1|\aleph(0)|^{\beta-1})\ldots \\ &(1-\gamma_1|\aleph(k-1)|^{\beta-1}) \\ &\vdots \end{aligned}$$

$$|\aleph(k)| \leq |\aleph(0)|(1-\gamma_1|\aleph(0)|^{\beta-1})^k \tag{8.15}$$

If $|\aleph(0)|(1-\gamma_1|\aleph(0)|^{\beta-1}) \leq \gamma_1|\aleph(k)|^{\beta}$, then from (8.15), $|\aleph(k)| \leq \gamma_1|\aleph(k)|^{\beta} \Rightarrow |\aleph(k+1)| = 0, \forall\ k \geq \left\lceil \log_{[1-\gamma_1|\aleph_0|^{\beta-1}]} \frac{\gamma_1^{\frac{1}{1-\beta}}}{|\aleph_0|} \right\rceil + 1$. Moreover, the settling time expression is given by $I(\aleph_0) \leq \left\lceil \log_{[1-\gamma_1|\aleph_0|^{\beta-1}]} \frac{\gamma_1^{\frac{1}{1-\beta}}}{|\aleph_0|} \right\rceil + 1$. Thus, it can be inferred that the absolute value of the switching function approaches zero within a finite number of time steps.

8.4 Results and Discussion

The simulation outcomes demonstrate the efficacy of two devised DSMC controllers. Employing parameters $\omega = 0.5$, $\gamma_1 = 0.5$, $\beta = 0.1$ and $c = [0.66; 1; 0.12]^T$, along with initial conditions and simulation parameters detailed in Table I. Fig 8.2a, Fig 8.2b, Fig 8.3a, Fig 8.3b and Fig 8.4 portrays the cumulative results for the RL1-based DSMC controller, while Fig 8.5a, Fig 8.5b, Fig 8.6a, Fig 8.6b and Fig 8.7 illustrates the cumulative results for the RL2-based DSMC controller. Additionally, Fig 8.8a, Fig 8.8b, Fig 8.9a, Fig 8.9b and Fig 8.10 presents a comparison between RL1, RL2, and prior work by Bandal et al. [76]. Notably, Bandal et al. using Gao's reaching law utilized quasi-sliding mode (QSM) with a band of 0.0625, depicted in Fig 8.3b and Fig 8.6b, whereas both RL1 and RL2 controllers exhibit an ideal sliding mode akin to CSMC. Fig 8.2a and Fig 8.5a represent the position versus time plot, showcasing precise attainment of the desired state x_{1d} (0.01m) for RL1 and RL2 within a finite time frame, respectively.

Furthermore, Fig 8.2b, Fig 8.3a and Fig 8.3b respectively demonstrate velocity, switching surface and current control input versus time plots for a RL1 based discrete-time sliding mode controller. Also, Fig 8.5b, Fig 8.6a and Fig 8.6b respectively demonstrate velocity, switching surface and current control input versus time plots for an RL2 based discrete-time sliding mode controller. The ferromagnetic ball achieves its desired steady-state position of 0.01 m in approximately 6.5 seconds, with the current stabilizing around 0.285 Amperes, near the targeted value of 0.2884 A with an RL1-based controller. Also with RL2-based controller ensures the desired steady-state position of 0.01 m in approximately 6.2 seconds, with the current stabilizing around 0.281 Amperes. The previous work shows minor oscillations around the desired values attributed to the quasi-sliding motion of the state trajectory, whereas RL1 and Rl2 based controller shows ideal sliding

motion along the surface.

8.5 Conclusions

This chapter introduces two DSMC control strategies for a magnetic levitation system. Its fast convergence rate characterizes DSMC based on RL1 and RL2 as compared to Gao's based control. These regulations tackle the constraints linked with Gao's reaching technique and Utkin's equivalent control method. With the proposed DSMC, the trajectory reaches a sliding surface, closely resembling its continuous-time counterpart without disturbances, thereby enhancing robustness. Moreover, DSMC proves more practical for magnetic levitation systems compared to previous DSMC-based control methods. The proposed laws for MLS successfully eliminate chattering while ensuring minimal control effort. Their effectiveness is supported by simulation results. Moving forward, the prospect of experimental validation using real-world setups presents an exciting opportunity for future research.

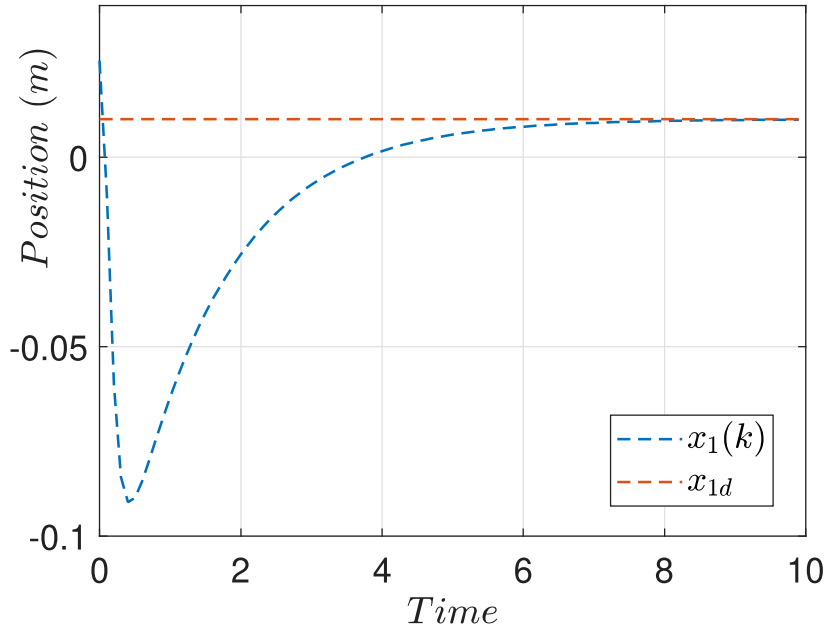

(a) RL1 state variable $x_1(k)$

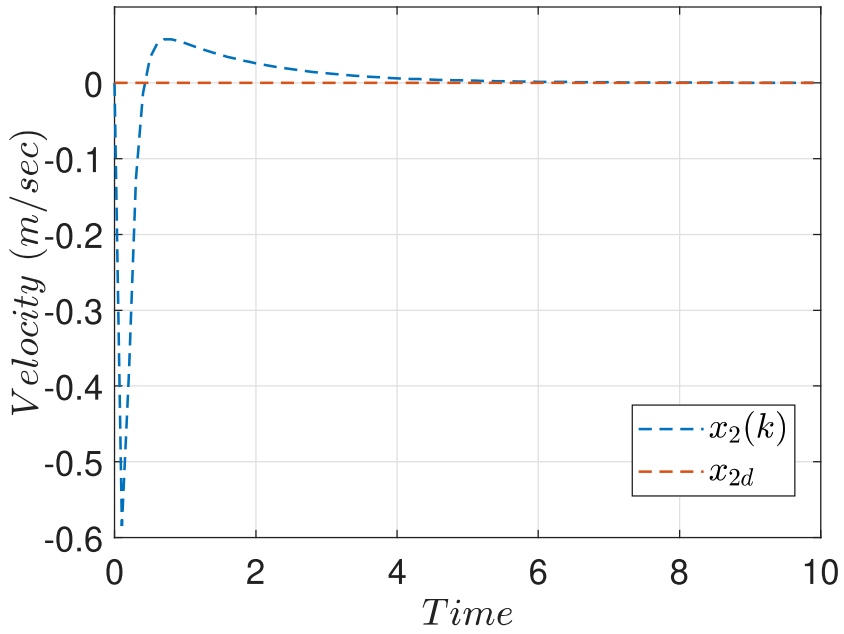

(b) RL1 state variable $x_2(k)$

Figure 8.2: RL1 State Variables

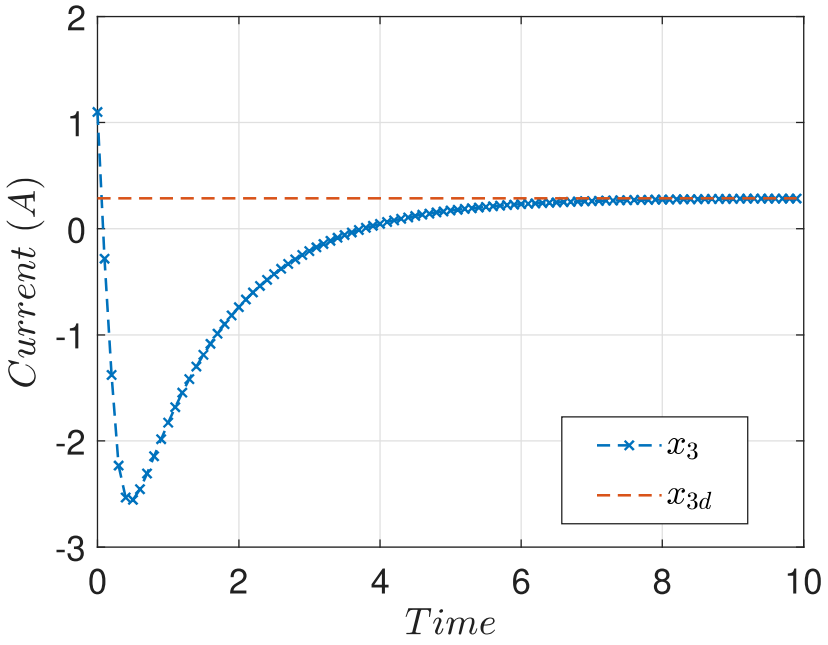

(a) RL1 state variable $x_3(k)$

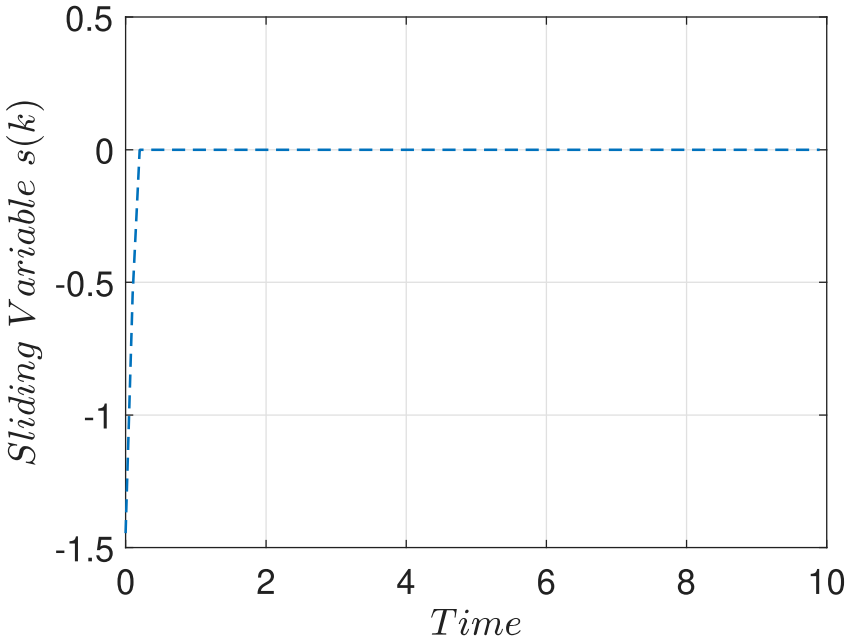

(b) RL1 sliding variable

Figure 8.3: RL1 State Variables and Sliding variable

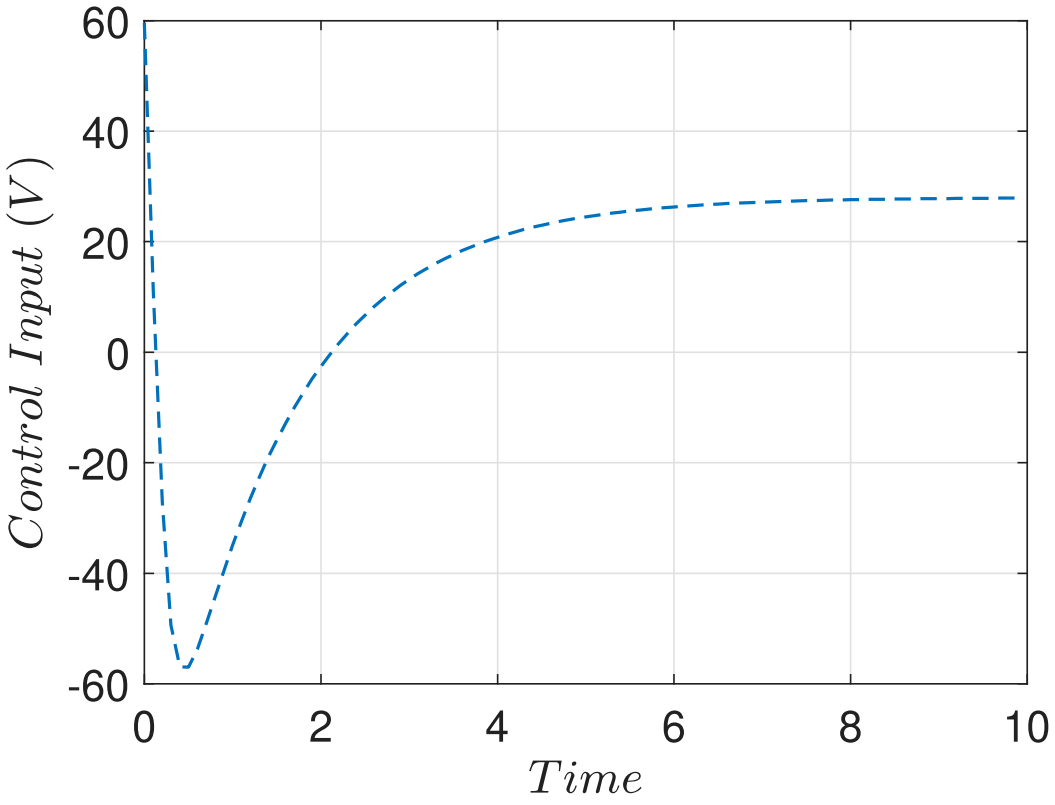

Figure 8.4: RL1 Control Input

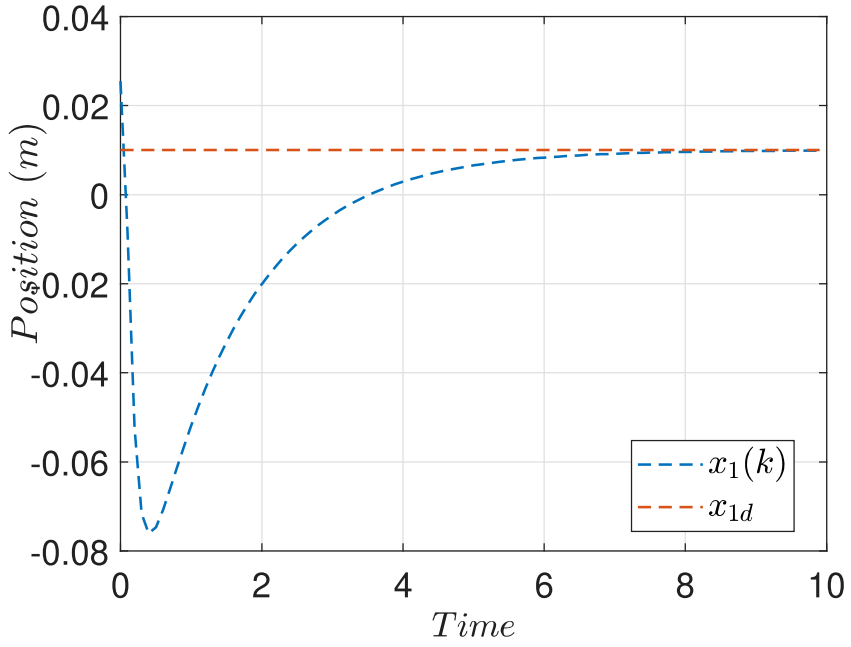

(a) RL2 state variable $x_1(k)$

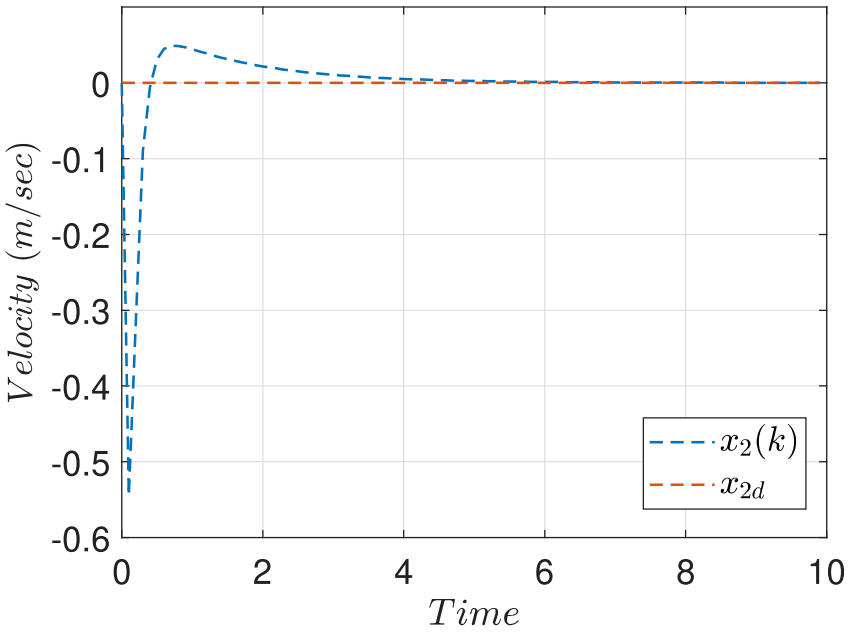

(b) RL2 state variable $x_2(k)$

Figure 8.5: RL2 State Variables

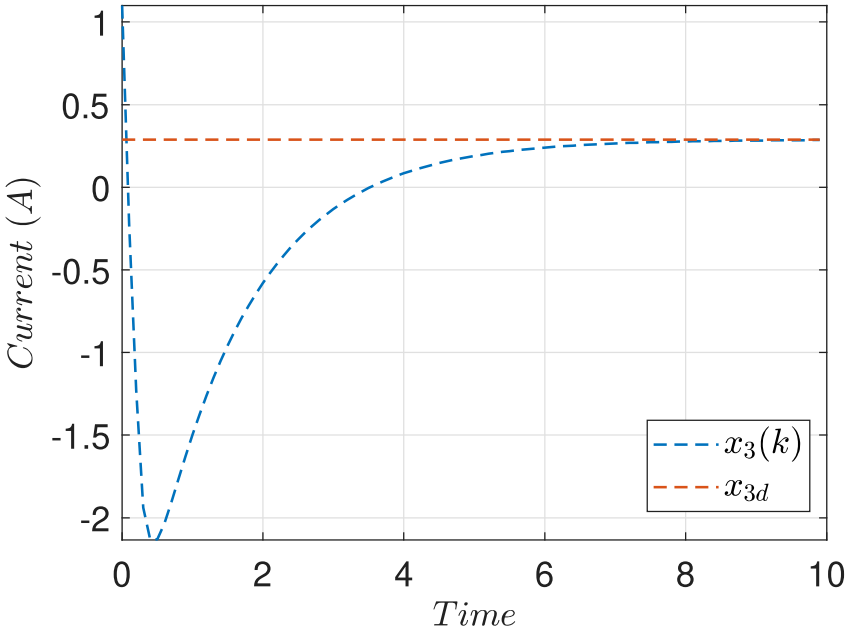

(a) RL2 state variable $x_3(k)$

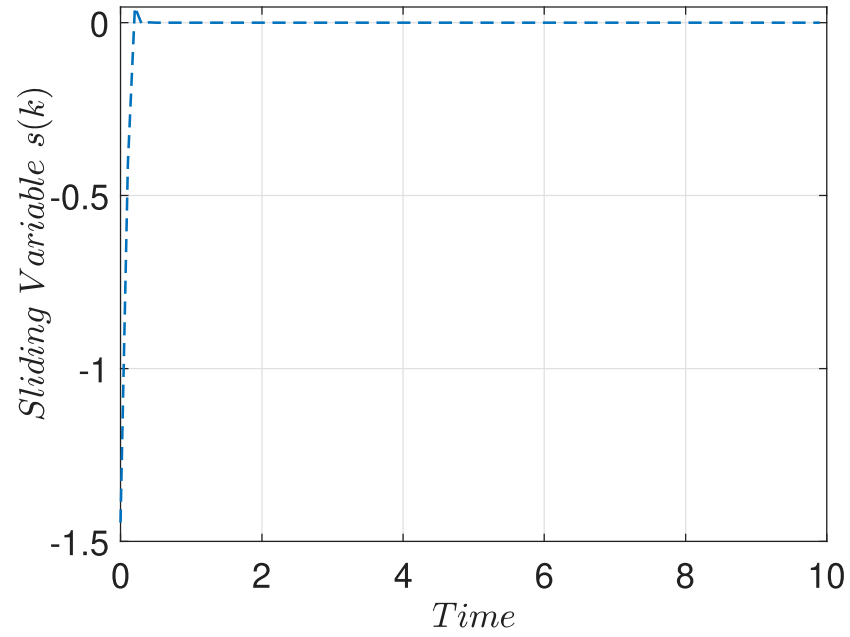

(b) RL2 sliding variable

Figure 8.6: RL2 State Variables and Sliding variable

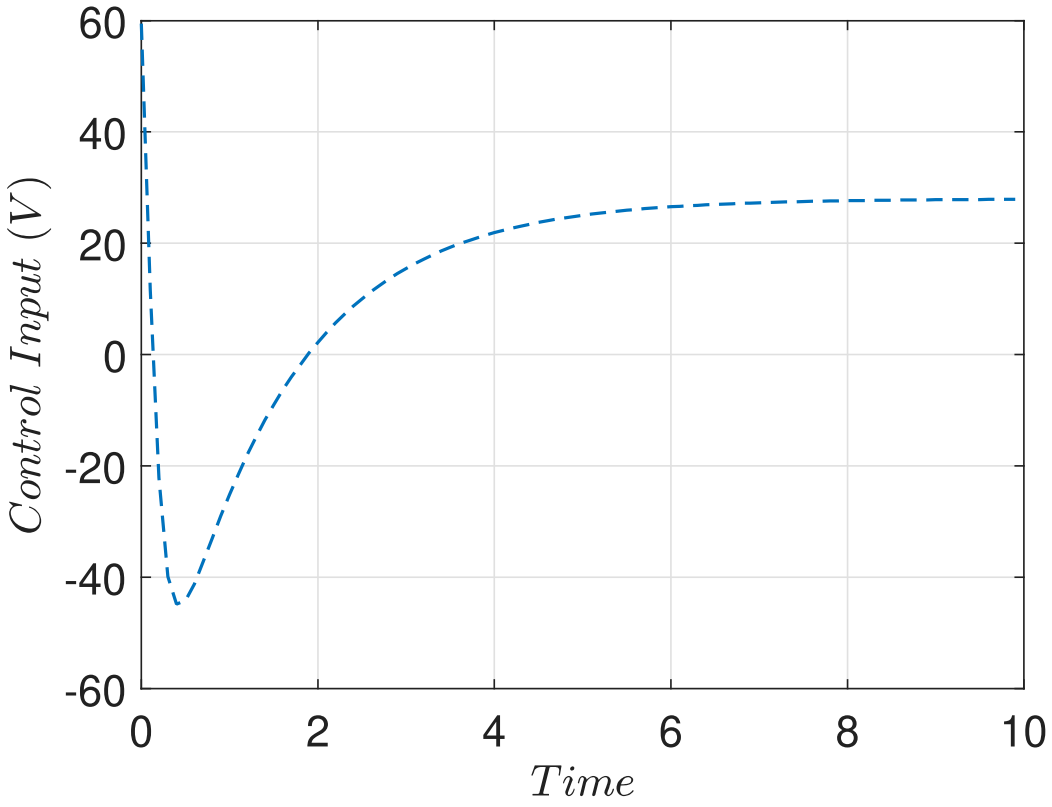

Figure 8.7: RL2 Control Input

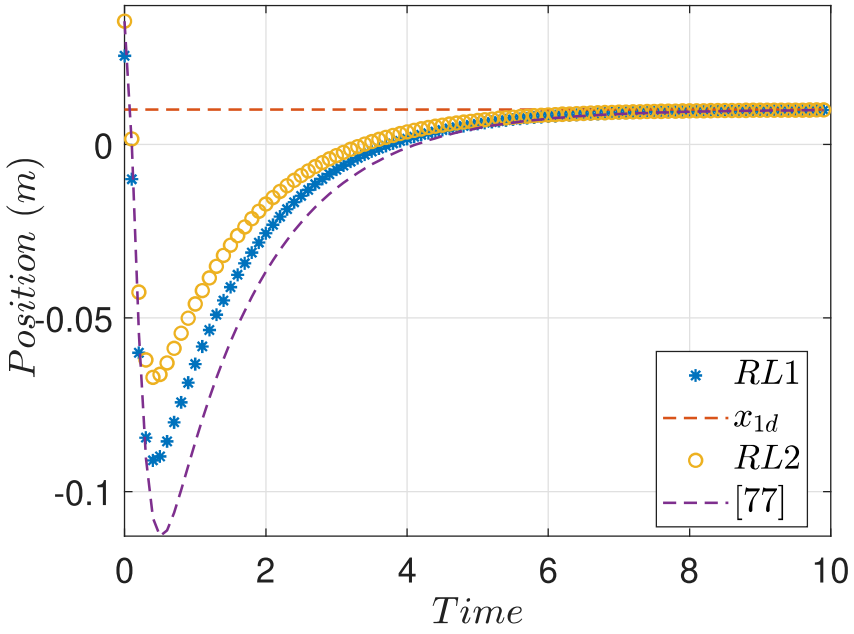

(a) Comparison state variable $x_1(k)$

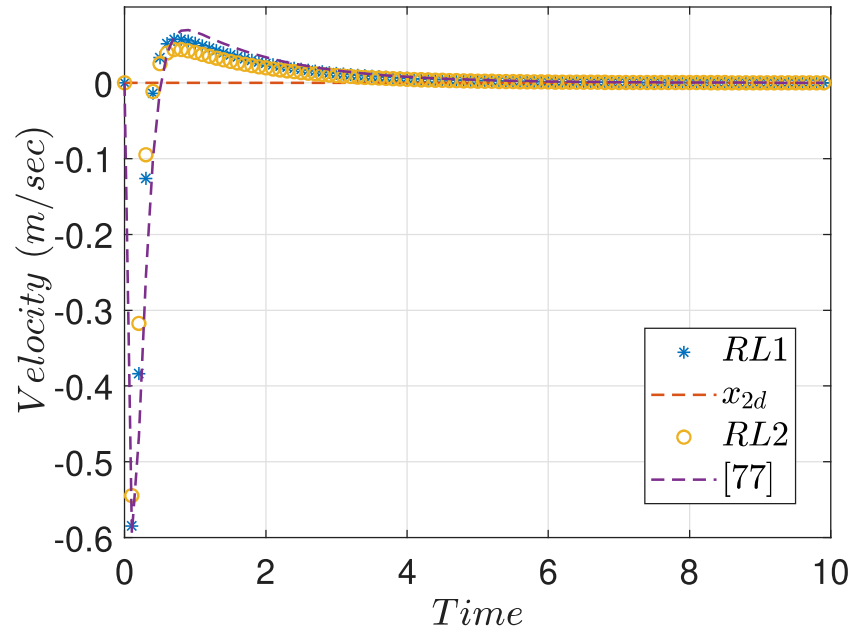

(b) Comparison state variable $x_2(k)$

Figure 8.8: RL1, RL2 and [77] Comparison

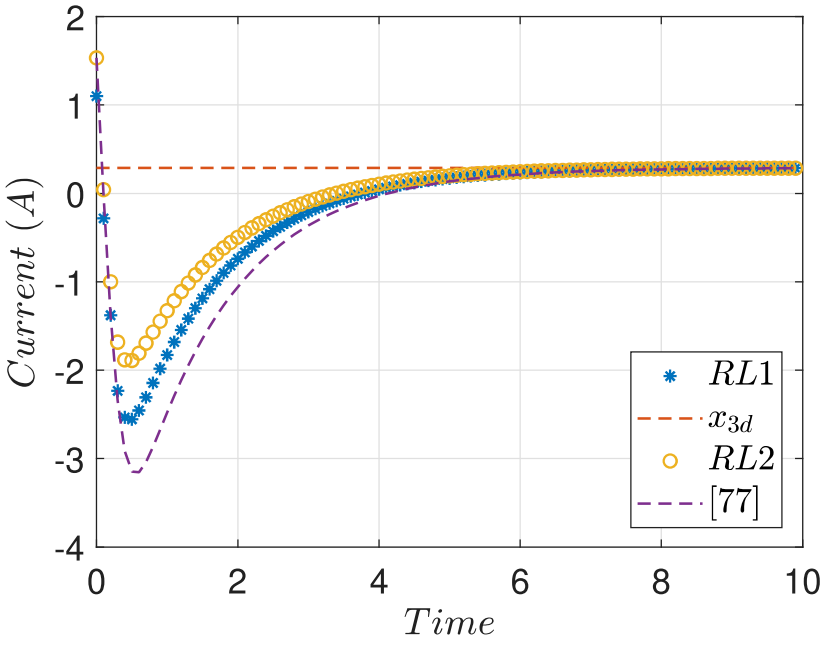

(a) Comparison state variable $x_3(k)$

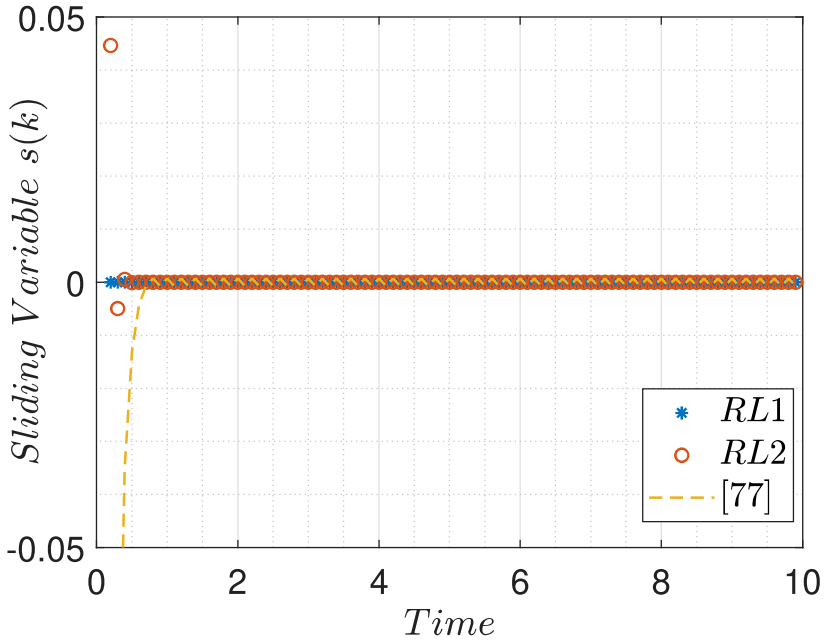

(b) Comparison sliding variable

Figure 8.9: RL1, RL2 and [77] Comparison

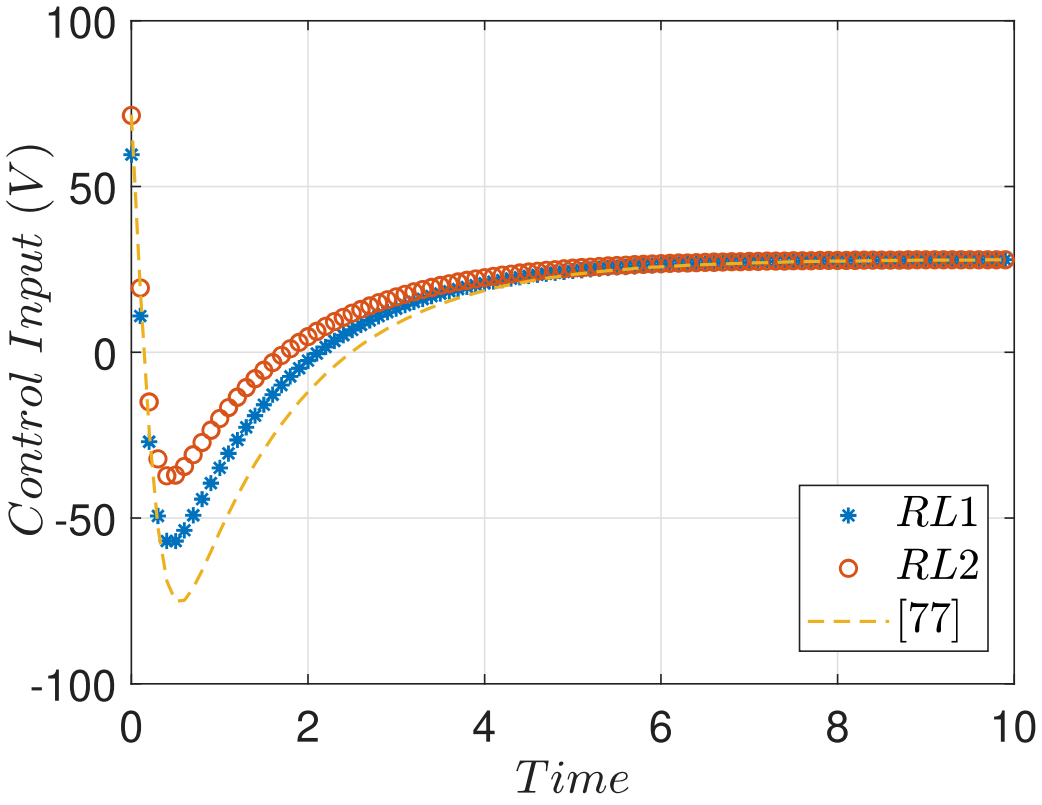

Figure 8.10: Comparison control input for RL1, RL2 and [77]